



Deformation behaviour and damage evolution of aluminium alloy sheet in electromagnetic forming with uniform pressure actuator

Xiaoyong Zeng¹ · Zhenghua Meng² · Wei Liu^{1,3,4} · Shangyu Huang^{1,3} · Shoulu Zhou¹ · Yangzhe Lin¹

Received: 27 November 2019 / Accepted: 30 June 2020 / Published online: 7 July 2020
© Springer-Verlag London Ltd., part of Springer Nature 2020

Abstract

Damage evolution has a great influence on the formability and mechanical property of part. The deformation behaviour and damage evolution of aluminium alloy sheet in the electromagnetic forming processes with uniform pressure actuator were experimentally and numerically investigated. The influences of the discharge voltage and impacting distance on the impacting effects between the aluminium alloy sheet and die wall were firstly compared in electromagnetic forming process. With the elevated discharge voltage and impacting distance, the impacting velocity and contacting pressure increased, and the stress triaxiality and damage accumulation of aluminium alloy sheet decreased. Then, the influences of the pre-straining level on the damage evolution of aluminium alloy sheet were presented in hybrid electromagnetic forming process. The initial damage of aluminium alloy sheet was accumulated during the quasi-static tensile pre-straining phase. The pre-strained specimens were subsequently electromagnetically formed, and the damage increment of aluminium alloy sheet can be suppressed with the higher pre-straining level.

Keywords Electromagnetic forming · Uniform pressure actuator · Damage

1 Introduction

Damage is an important factor for the deformation behaviour and formability in sheet metal forming. The investigation into damage evolution provided great potentials to predict the forming limits, especially in the case of new categories of sheet metals and innovative forming processes [1]. In addition, the damage involved in the plastic forming is significant for predicting and setting the mechanical property of formed parts [2]. The damage accumulation can be decreased by the specific design of forming processes, such as the

superposition of compressive stresses, to increase the fatigue strength of the component in service [3].

Electromagnetic forming (EMF) is one of high-speed forming processes, in which the intensive Lorentz force is instantaneously generated by the eddy current to form tubes or sheets [4]. It exhibits the advantages of higher formability, lower springback, no contact, less residual stress and so on. Therefore, EMF has indicated the great potential for application in sheet metal forming, especially when it is combined with the other conventional forming technology [5]. Imbert et al. [6] investigated the effect of tool-sheet interaction on damage evolution of aluminium alloy sheet by comparing the free form and conical die bulging experiments. The forming-induced damage can be suppressed by the tool-sheet interaction due to the stress state changing, and the nucleation strain shows a significant influence on the damage evolution. Imbert et al. [7] adopted the hybrid EMF process to reduce a pre-formed radius of aluminium alloy sheet. The high compressive hydrostatic stress and the highest strain rates were supposed to increase the formability. Kim et al. [8] compared the V-shaped bending processes of the conventional stamping and EMF. They assumed that the formability is improved mainly by suppressing the damage due to the impact of the sheet with the die. Zou et al. [9] numerically investigated

✉ Wei Liu
weiliu@whut.edu.cn

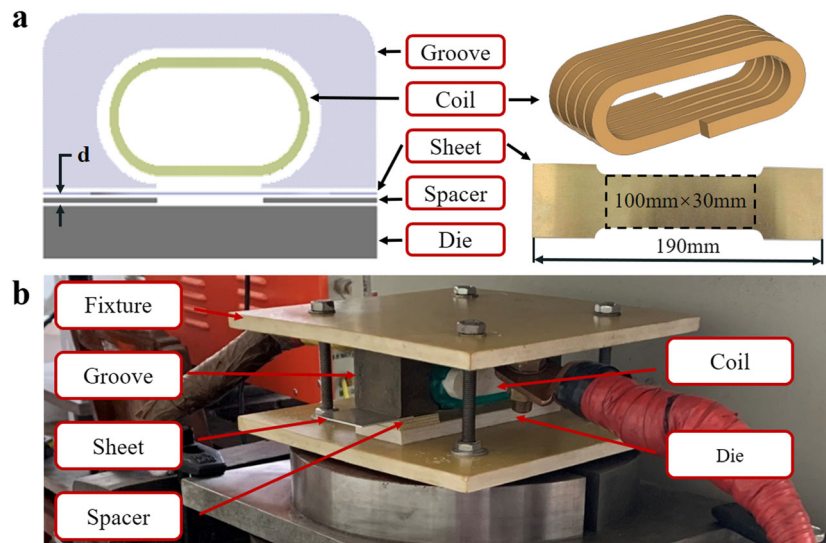
¹ School of Materials Science and Engineering, Wuhan University of Technology, Wuhan 430070, China

² School of Automotive Engineering, Wuhan University of Technology, Wuhan 430070, China

³ Hubei Engineering Research Center for Green Precision Material Forming, Wuhan University of Technology, Wuhan 430070, China

⁴ State Key Laboratory of Materials Processing and Die & Mould Technology, Huazhong University of Science and Technology, Wuhan 430070, China

Fig. 1 Experimental unit of EMF with UPA



the influence of the discharge voltage on the damage evolution in the electromagnetic bulging with a conical die. The damage of aluminium alloy sheet can be reduced more significantly with the higher voltage. In the literatures, the damage accumulation can be suppressed in the EMF processes when the sheet metals impact with the die wall at very high speed, and it is considered as a main factor for the much higher formability. Furthermore, the EMF shows the possible prospects for setting the product property due to the damage suppression, especially for the hybrid EMF processes in which the pre-straining stage may result in the initial damage accumulation. Hence, it is necessary to investigate the process parameters of EMF on the damage evolution of sheet metals.

In EMF, the deformation behaviour of sheet metals is immensely dependent on the design of coil structure. Due to the non-uniform electromagnetic forces induced by the flat spiral coil, it brings about the heterogeneous deformation of sheet metals. Hence, Kamal et al. [10] proposed a uniform pressure actuator (UPA) to obtain homogeneous electromagnetic forces for EMF of sheet metals. Due to the high impacting velocity and pressure induced by the UPA, Golowin et al. [11]

applied it for shock hardening to significantly increase the hardness of sheets. Thibaudeau et al. [12] developed an analytical model of UPA for EMF and magnetic pulsed welding (MPW). Meng et al. [13] adopted the UPA for electromagnetic forming of magnesium alloy sheets at elevated temperatures. The effects of discharged voltage and temperature on the bulging height were experimentally investigated. Feng et al. [14] showed the uniform electromagnetic forces of UPA and deformation distribution of magnesium alloy sheet during the electromagnetic bulging process. Xu et al. [15] found that the formability of magnesium alloy sheet is improved by using UPA and aluminium alloy driver sheet of 1 mm thickness at higher discharge energy and warm temperature. Kim et al. [16] suggested that the distance between the UPA and sheet, the wire thickness and the distance between the wires should be as small as possible for electromagnetic bulging of aluminium alloy sheets. On the basis of the electromagnetically assisted stamping (EMAS) presented by Shang et al. [17], Liu et al. [18] designed a dedicated UPA for EMAS of a surface part of aluminium alloy sheet. The influence of discharge voltages on the springback reduction was investigated to improve the forming accuracy of the part. Therefore, the UPA shows the distinct advantage of uniform electromagnetic forces and exhibits a good potential for application into the EMF or hybrid EMF processes.

With the concern of setting product property beyond shaping, the deformation behaviour of aluminium alloy sheet in the EMF with UPA was experimentally and numerically investigated. The influence of the discharge voltage, the impacting

Table 1 The parameters of GTN model [6]

Parameters	Value
q_1	1.5
q_2	1.0
Initial void volume fraction f_0	0.0
Initial void nucleating particle fraction f_N	0.03
Average nucleation strain ε_N	0.05
Standard deviation of nucleation strain s_N	0.01
Coalescence void volume fraction f_C	0.03
Failure void volume fraction f_F	0.2

Table 2 The parameters of Cowper–Symonds hardening model [20]

k	n	C	P
345 MPa	0.148	7000 s ⁻¹	0.96

distance and the pre-straining level on the damage evolution was inspected by numerical simulation. The results can provide several fundamentals for EMF process design with UPA.

2 Experimental and simulation schemes

2.1 Experimental procedures

The experimental unit of EMF with UPA is shown Fig. 1. It mainly consists of the groove, the coil, the sheet, the spacer and the die, as shown in Fig. 1a. The groove is made of aluminium alloy for combining with the sheet to induce eddy current return. The conventional UPA of rectangular helical coil was used, of which the winding number is five, the winding section is 6 mm × 6 mm and the winding distance is 2 mm. It was made of red copper and embedded into a polytetrafluoroethylene mandrel to resist the electromagnetic force. The AA5754 aluminium alloy sheet with the thickness of 1 mm was chosen for specimens. The length and width of measurement zone are 110 mm and 30 mm. The specimen is accelerated by the opposed Lorentz forces induced by the eddy current. The distance *d* between the sheet and die can be changed by the thickness of spacer, so the impacting condition between the sheet and die can be conveniently controlled.

The EMF experiment was carried out with the EMF machine at Wuhan University of Technology. The maximum energy is 60 kJ, the maximum storage capacitor is 1100 μF and the maximum voltage is 11 kV. Here, the capacitance was chosen as 550 μF. The experimental unit was clamped into two insulating plates with screws, as show in Fig. 1b. The circle grids were printed on the specimen for optical measurement of deformation. The pre-straining phase was performed under quasi-static tensile condition with the Instron testing machine. The pre-straining level was measurement by an extensometer.

2.2 Numerical modelling

The commercial software LS-DYNA and the electromagnetic module EM were used for numerical simulation. The electromagnetic field and the deformation of the sheet were sequentially coupled by finite element method, and the electromagnetic field in the surrounding air was considered by the boundary element method to reduce the computation cost. In order to predict the damage evolution, the Gurson–Tvergaard–Needleman (GTN) damage model is used to represent the mechanical behaviour of AA5754 aluminium alloy sheet. The void volume fraction is used as the damage index in the GTN model as follows [19]:

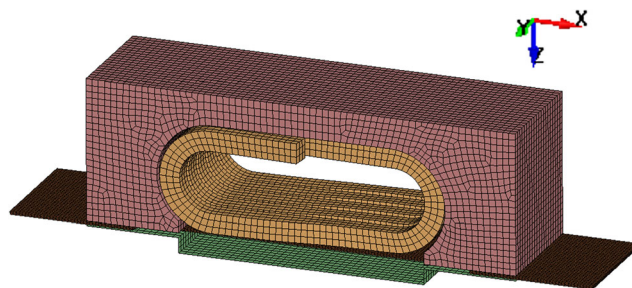


Fig. 2 The numerical model of EMF

$$\phi = \frac{\sigma_M^2}{\bar{\sigma}} + 2q_1 f^* \cosh\left(\frac{3q_2 \sigma_H}{2\bar{\sigma}}\right) - 1 - (q_1 f^*)^2 = 0 \quad (1)$$

where σ_M is the von Mises equivalent stress, $\bar{\sigma}$ is the yield stress and σ_H is the mean hydrostatic stress. The effective void volume fraction is defined as

$$f^*(f) = \begin{cases} f & f \leq f_c \\ f_c + \frac{1}{f_F - f_c} (f - f_c) & f > f_c \end{cases} \quad (2)$$

The growth of void volume fraction is defined as

$$\dot{f} = \dot{f}_G + \dot{f}_N \quad (3)$$

where the growth of existing voids and the nucleation of new voids are defined as

$$\dot{f}_G = (1-f) \dot{\epsilon}_{kk}^p \quad (4)$$

$$\dot{f}_N = A \dot{\epsilon}_p \quad (5)$$

$$A = \frac{f_N}{S_N \sqrt{2\pi}} \exp\left[-\frac{1}{2} \left(\frac{\epsilon_p - \epsilon_N}{S_N}\right)^2\right] \quad (6)$$

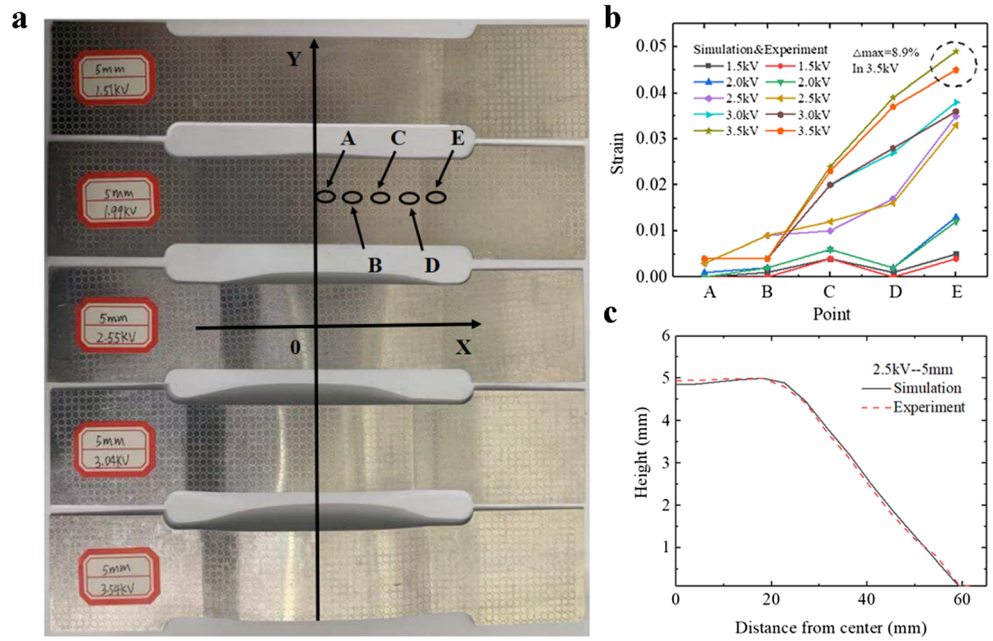
The new voids are nucleated only in tension. The parameters of the GTN model are shown in Table 1.

The density of AA5754 aluminium alloy sheet is 2780 kg m⁻³. The Young’s modulus and Poisson’s ratio are 70 GPa and 0.33. The hardening behaviour is described with the Cowper–Symonds model as follows:

Table 3 The electrical parameters [18]

Category	Parameters	Value
RLC circuit	Resistance (mΩ)	15
	Inductance (μH)	3
	Capacitance (μF)	550
	Groove (MS m ⁻¹)	36
Electrical conductivity	Sheet (MS m ⁻¹)	36
	Coil (MS m ⁻¹)	58

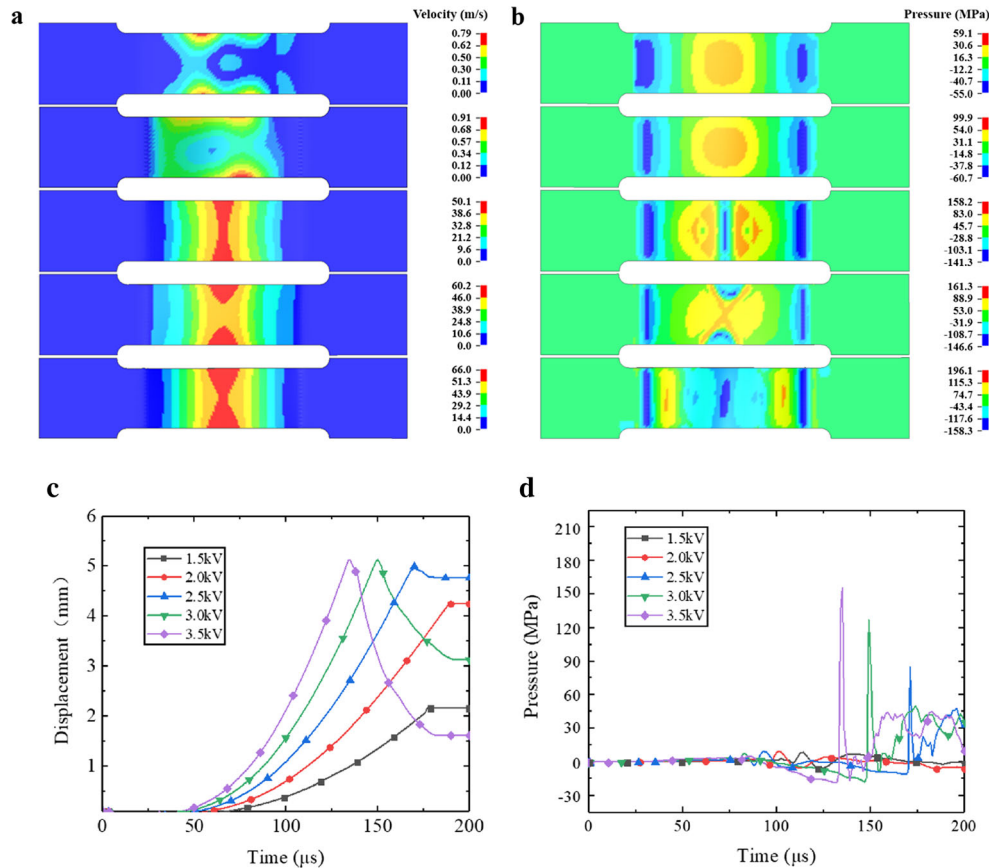
Fig. 3 The results under different discharge voltages: **a** specimens, **b** strains of simulation and experiment, and **c** profiles of simulation and experiment



$$\bar{\sigma} = \left(k \bar{\epsilon}_p^n \right) \left[1 + \left(\frac{\dot{\epsilon}}{C} \right)^P \right] \quad (7)$$

where $\bar{\epsilon}_p$ is the plastic strain, $\dot{\epsilon}$ is the strain rate, k is the strength coefficient, n is the hardening exponent and C and P are strain-rate-dependent hardening parameters. The parameters of the Cowper–Symonds hardening model are shown in Table 2.

Fig. 4 The velocity and pressure under different discharge voltages: **a** impacting velocity, **b** impacting pressure, **c** displacement curves, and **d** pressure curves



In the numerical model, the sheet is meshed with the hexahedral solid elements for the eddy current. There are three layers of elements along the thickness direction. The groove, the coil, the spacer and the die are defined to be rigid, as shown in Fig. 2. The electrical parameters of RLC and materials are shown in Table 3. The contact conditions between the groove, spacer and sheet are respectively defined. The time increment steps for coupling the magnetic and deformation are both $1 \mu\text{s}$. The total time of EMF simulation is $200 \mu\text{s}$.

3 Experimental and simulated results

3.1 Influence of discharge voltage on deformation behaviour and damage evolution

Different discharge voltages of 1.5 kV, 2.0 kV, 2.5 kV, 3.0 kV, and 3.5 kV were applied to deform the specimens under the constant impacting distance $d = 5 \text{ mm}$, and the deformed specimens are as shown in Fig. 3a. When the discharge voltages were 1.5 kV and 2.0 kV, the specimens only endured the deformation caused by the Lorentz Forces and did not contact with the die wall. When the discharge voltages were above 2.5 kV, the deformation of specimens was large enough to impact the die wall. With the higher discharge voltages, the rebound occurred at the central region of specimen after impacting.

The strains along the X direction were compared between the experiment and simulation at the points of A, B, C, D, and E, as shown in Fig. 3b. When the discharge voltage increases, the deformation level of specimen rises up. The strains at the point A are the smallest, while the ones at the point E near the edge of die are the largest. The simulated strains nearly coincide with the experimental ones. The maximum relative error was 8.9% and occurred at the point E. The error may be caused by the complex contact conditions near the edge of die in the simulation and the large strain measurement in the experiment. As an example, the simulated and experimental profiles of part under the discharge voltage of 2.5 kV and the impacting distance of 5 mm were compared in Fig. 3c. It was found that the profiles nearly coincided with each other.

The impacting velocity and pressure of specimens under different discharged voltages were compared in Fig. 4. When the discharge voltage is lower than 2.0 kV, the specimens cannot contact with the die wall. Due to the low discharge energy, the velocity of specimens decreased very quickly with the deformation and it became to be zero before impacting with the die, as shown in Fig. 4a. The pressure on the central region of specimen was caused only by the impulse magnetic pressure, as shown in Fig. 4b. When the discharge voltage is higher than 2.5 kV, the discharge energy is

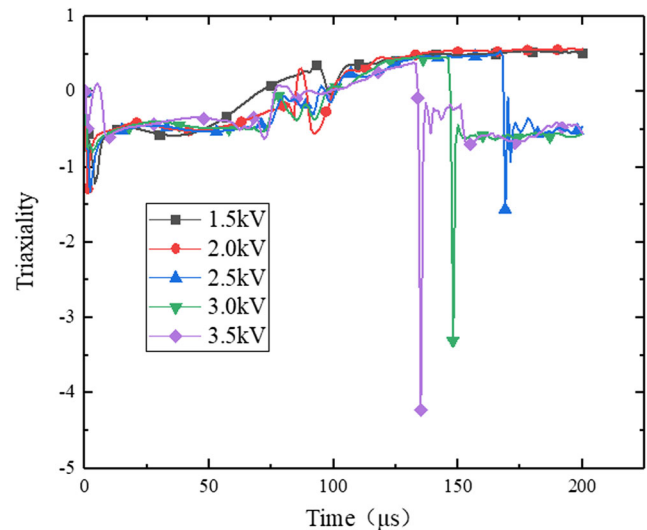


Fig. 5 The curves of stress triaxiality

enough to deform the specimens and push them to impact the die wall. When the specimens just impacted with die, the impacting velocity is still higher than 50 m/s. Therefore, besides the impulse magnetic pressure, the reacting pressure occurred on the central region of specimen because of impacting with the die. The impacting pressure is high as 158.3 MPa when the discharged voltage is 3.5 kV. The displacement and pressure curves at the central point A under different discharge voltages were shown in Fig. 4 c and d. It can be seen that the impacting pressure is higher for 3.0 kV and 3.5 kV, but the rebound displacement is larger. When the discharge voltage is 2.5 kV, the rebound displacement is very small and the pressure is about 90 MPa.

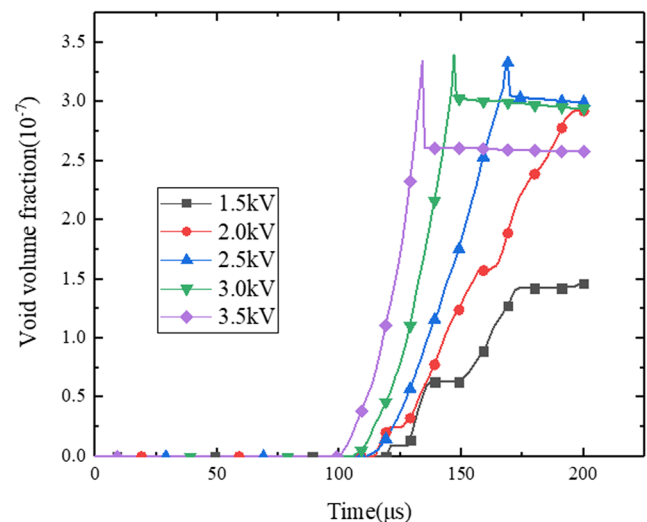
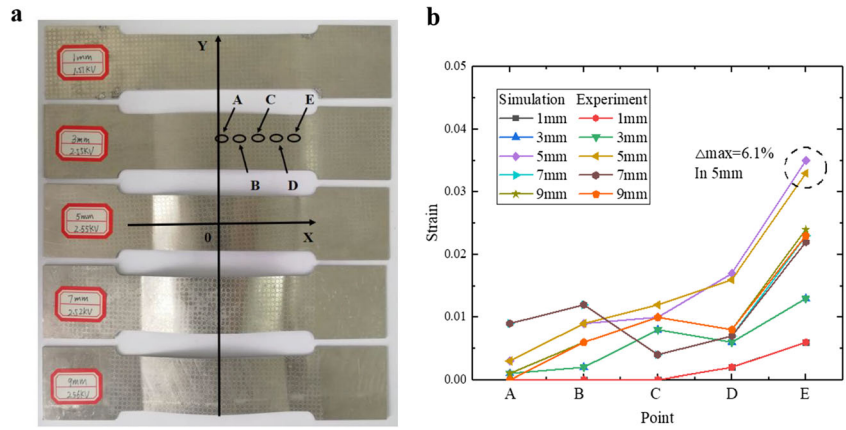


Fig. 6 The curves of void volume fraction

Fig. 7 The results under different impacting distances: **a** specimens and **b** strains of simulation and experiment



The curves of stress triaxiality (defined as the ratio of hydrostatic stress and von Mises equivalent stress) at the point A under different discharged voltages were compared in Fig. 5. It can be seen that the stress triaxiality decreased abruptly when the specimen impacted with the die wall under the discharge voltage of above 2.5 kV. The proportion of hydrostatic stress is larger with the higher discharge voltage. The evolutions of void volume fraction at the point A under different discharged voltages were shown in Fig. 6. The void volume fraction of specimen increased under the discharged voltages of 1.5 kV and 2.0 kV, while the void volume fraction of specimen initially increased with the positive stress triaxiality and subsequently decreased due to the significant negative stress triaxiality under the discharged voltages above 2.5 kV. Hence, the damage will be induced in the EMF processing but can be suppressed by impacting with the die under higher discharged voltage.

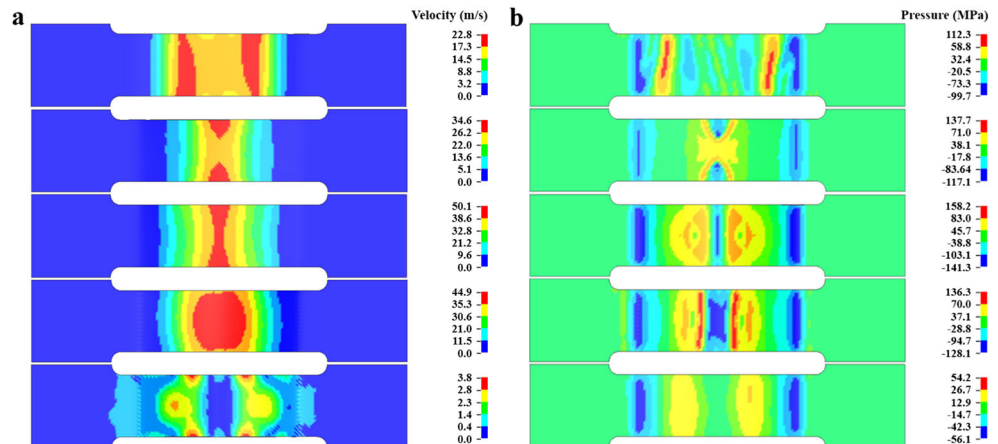
3.2 Influence of impacting distance on deformation behaviour and damage evolution

Different impacting distances of 1 mm, 3 mm, 5 mm, 7 mm, and 9 mm between the specimen and die were initially

changed by the different thickness of spacers. The discharge voltage was fixed to be 2.5 kV. The specimen impacted with the die wall under the impacting distances of 1 mm, 3 mm, 5 mm, and 7 mm, while the specimen did not contact with the die wall under the distances of 9 mm, as shown in Fig. 7a. When the impulse forces came to end, the velocity of specimen decreased with the deformation increasing. If the distance between the specimen and die was too large, the velocity of specimen became to be zero without contacting with the die wall.

The experimental and simulated strains at the points of A, B, C, D, and E along the X direction were compared in Fig. 7b. The deformation at the point A became larger when the impacting distance was changed from 1 to 7 mm. However, the deformation at the point A was very small when the distance is 9 mm. The deformation level at the central region of specimen was obviously changed during the impacting process. Meanwhile, the strain distribution became a little complex due to the rebound of specimen after impacting. The largest strains also occurred at the point E near the edge of die. It showed a relatively good agreement between the simulated and experimental strains.

Fig. 8 The impacting velocity and pressure under different impacting distances: **a** velocity and **b** pressure



The impacting velocity and pressure of specimens under different impacting distances were compared in Fig. 8. When the impacting distance ranged from 1 to 5 mm, the impacting velocity increased up to 50.1 m/s, and the impacting pressure rises up to 158.2 MPa at the central point. However, the impacting velocity and the impacting pressure became a little lower when the impacting distance was 7 mm, because the kinematic energy of sheet decreased to promote the deformation. When the distance is 9 mm, the velocity of specimen became zero so that it cannot contact with the die wall. Hence, there was no impacting pressure at the central region. If the impacting distance was too small, the impacting velocity and pressure were not high enough. If the impacting distance was too large, the impacting velocity and pressure would decrease, and even become zero before contacting with the die wall.

The curves of stress triaxiality at the point A under different impacting distances were compared in Fig. 9. It can be seen that the stress triaxiality was abruptly changed several times under the impacting distances of 1 mm and 3 mm because of the rebound after impacting with the die wall. However, the void volume fraction was very small, as shown in Fig. 10. When the impacting distance was 5 mm, the stress triaxiality was abruptly changed only one time. The void volume fraction initially increased due to the bulging deformation and then decreased a very little after impacting with the die wall. Although the sheet impacted with the die under the impacting distance of 7 mm, the void volume fraction only increased with the bulging deformation and did not decrease because the hydrostatic stress was not significant. The void volume fraction was highest when the distance between the sheet and die was 9 mm.

3.3 Influence of pre-straining level on deformation behaviour and damage evolution

The specimens were preformed under the quasi-static uniaxial tension to reach the pre-straining levels of 0.2%, 2.0%, 5.0%, and 8.0%, and then these specimens were deformed in EMF under the discharge voltage of 2.5 kV and the impacting distance of 7 mm. The preformed specimens were compared with the undeformed one in Fig. 11a, and the initial void volume fractions were predicted by numerical simulation, as shown in Fig. 11b. The damage accumulation of specimen became more significant with the elevated pre-straining levels under the uniaxial tensile conditions. The formed specimens and the strains were also compared in Fig. 11 c and d. The specimens compacted with the die wall during the EMF phase. The strains

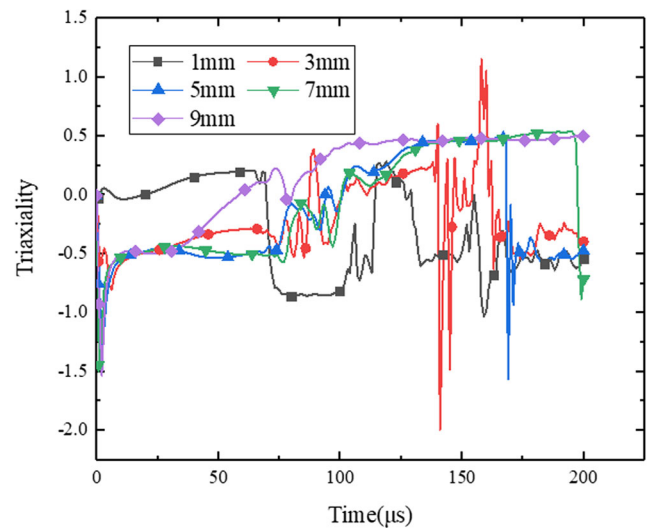


Fig. 9 The curves of stress triaxiality

induced by EMF were very little when compared with the pre-straining levels.

The impacting velocity of specimens under different pre-straining levels was shown in Fig. 12a, and the impacting velocity became a very little smaller with higher pre-straining levels due to the pre-straining hardening effect of specimens. The velocity is mainly determined by the inertial effect, because the impacting distance of 7 mm is not too large. The maximum velocity occurred at the central region of specimen, so the central region impacted with the die wall at the beginning. Hence, the impacting pressure initially occurred at the central region of specimen, as shown in Fig. 12b. Because the impacting velocities were nearly the same, the impacting pressures showed the similar tendency.

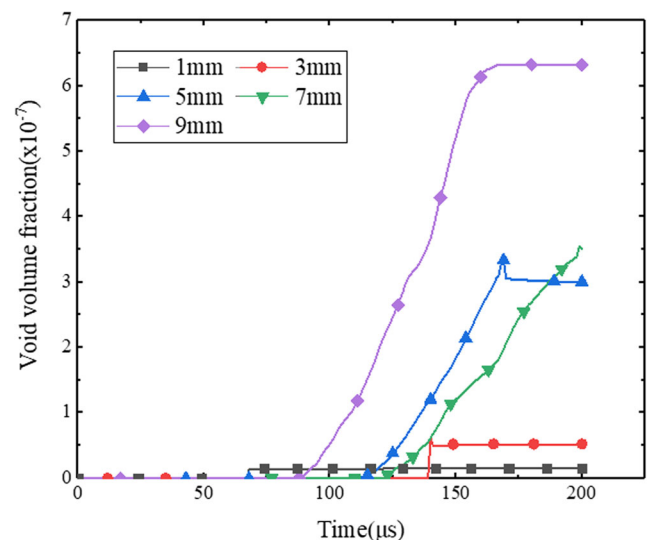
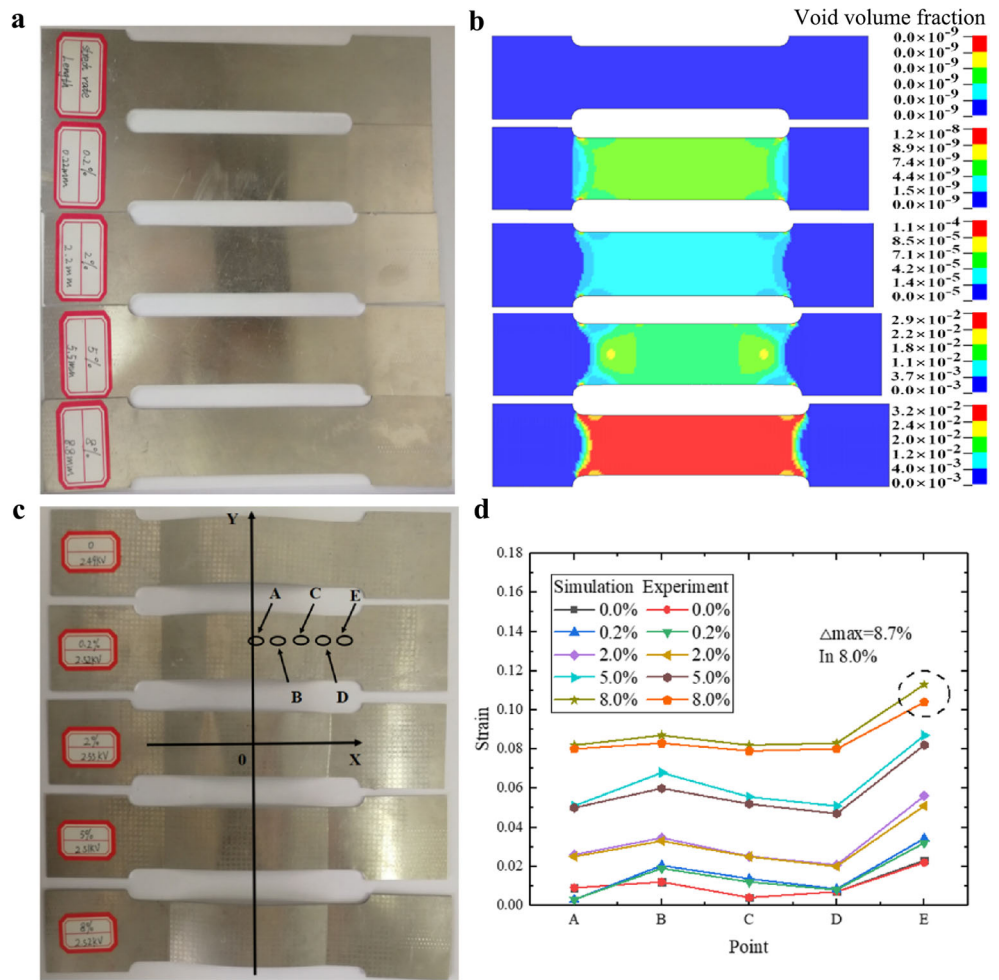


Fig. 10 The curves of void volume fraction

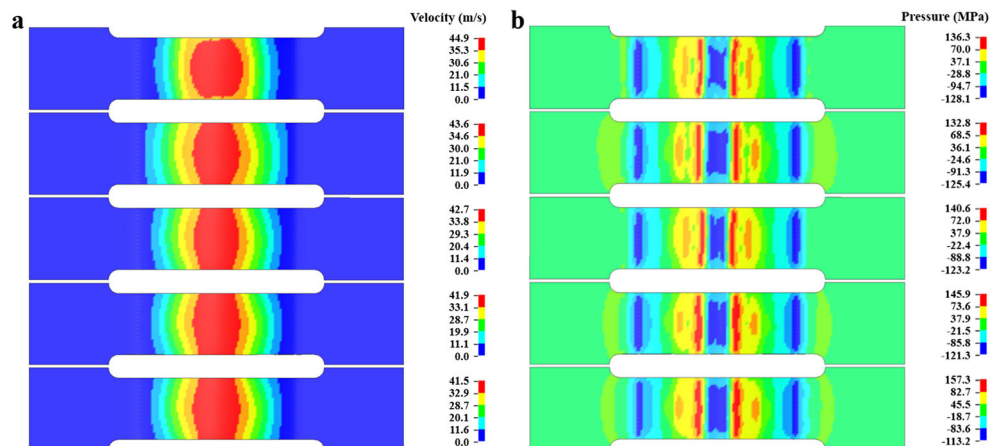
Fig. 11 The results under different pre-straining levels: **a** preformed specimens, **b** initial void volume fractions, **c** formed specimens, and **d** strains of simulation and experiment



The curves of stress triaxiality during the EMF phase under different pre-straining levels were shown in Fig. 13. It can be seen that all of the stress triaxiality

abruptly changed at the time of 196 μ s, because the impacting conditions were nearly the same. However, the curves of void volume fraction increment during

Fig. 12 The impacting velocity and pressure under different pre-straining levels: **a** velocity and **b** pressure



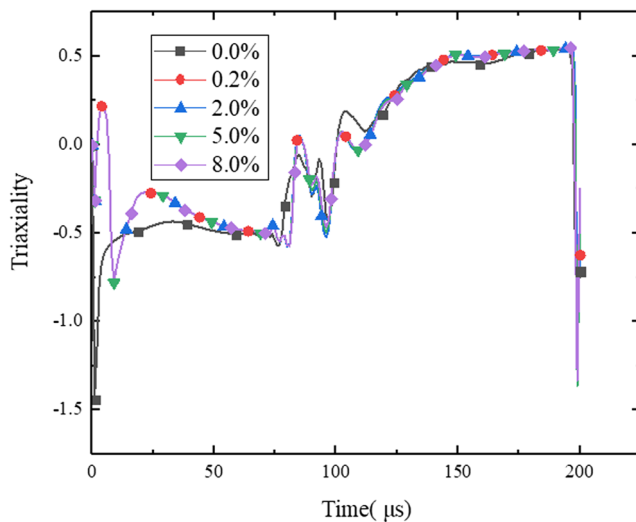


Fig. 13 The curves of stress triaxiality

the EMF phase were different, as shown in Fig. 14. The void volume fraction increments nearly remained to be zero under the pre-straining levels of 0%, 0.2% and 2.0%, while the void volume fraction increments initially increased due to the bulging deformation and subsequently decreased because of impacting with the die wall under the pre-straining levels of 5% and 8%. Finally, the void volume fraction became a little smaller than zero. The damage of specimens was not increased and even suppressed at some degree after the EMF phase under the higher pre-straining levels. When the higher pre-straining levels induced the more significant void volume fraction, it is more remarkable to exhibit the advantage of EMF to suppress the damage of formed part.

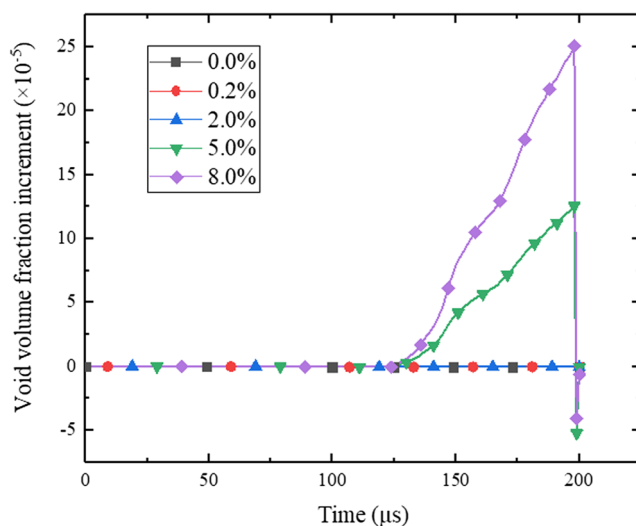


Fig. 14 The curves of void volume fraction

4 Conclusion

The influences of the discharge voltage, the impacting distance, and the pre-straining level on the deformation behaviour and damage evolution of aluminium alloy sheet during the EMF with UPA were experimentally and numerically investigated. The discharge voltage and the impacting distance have great effects on the impacting velocity and pressure. The impacting velocity and pressure increase with the higher discharged voltage, and a reasonable impacting distance should be determined to obtain the maximum impacting velocity and pressure. The higher impacting velocity and pressure can significantly reduce the stress triaxiality and suppress the damage induced by the deformation. The pre-straining level hardly has effect on the impacting condition but can make an effect on the damage of specimen in EMF process. With the higher initial void volume fraction, the effect of EMF to suppress the damage of part is more remarkable.

The EMF has shown great potentials in the aluminium alloy sheet forming, especially when it is combined with the conventional forming processes to put forward the hybrid EMF. Here, it is validated to suggest the perspectives to set the product properties beyond shaping by EMF or hybrid EMF. These results can provide some principals for the process design of EMF and hybrid EMF to suppress the damage of parts.

Funding information This project (2019CFB196) was supported by Natural Science Foundation of Hubei Province, China. We also would like to express our appreciation for the financial support from State Key Laboratory of Materials Processing and Die & Mould Technology (P2018-013, Huazhong University of Science and Technology, China), and Jiangsu Key Laboratory of Precision and Micro-manufacturing Technology (Nanjing University of Aeronautics and Astronautics, China).

References

1. Bruschi S, Altan T, Banabic D, Bariani PF, Brosius A, Cao J, Ghiotti A, Khraisheh M, Merklein M, Tekkaya AE (2014) Testing and modelling of material behaviour and formability in sheet metal forming. *CIRP Ann Manuf Technol* 63:727–749
2. Tekkaya AE, Allwood JM, Bariani PF, Bruschi S, Cao J, Gramlich S, Groche P, Hirt G, Ishikawa T, Löbbecke C, Lueg-Althoff J, Merklein M, Misiolek WZ, Pietrzyk M, Shivpuri R, Yanagimoto J (2015) Metal forming beyond shaping: predicting and setting product properties. *CIRP Ann Manuf Technol* 64:629–653
3. Tekkaya AE, Ben Khalifa N, Hering O, Meya R, Myslicki S, Walther F (2017) Forming-induced damage and its effects on product properties. *CIRP Ann Manuf Technol* 66:281–284
4. Psyk V, Risch D, Kinsey BL, Tekkaya AE, Kleiner M (2011) Electromagnetic forming—a review. *J Mater Process Technol* 211: 787–829

5. Li L, Li J, Wan M, Yu H, Liu L (2018) Innovation applications of electromagnetic forming and its fundamental problems. *Procedia Manuf* 15:14–30
6. Imbert JM, Winkler SL, Worswick MJ, Oliveira DA, Golovashchenko S (2005) The effect of tool-sheet interaction on damage evolution in electromagnetic forming of aluminum alloy sheet. *J Eng Mater Technol* 127:145–153
7. Imbert J, Worswick M (2012) Reduction of a pre-formed radius in aluminium sheet using electromagnetic and conventional forming. *J Mater Process Technol* 212:1963–1972
8. Kim J, Noh HG, Song WJ, Kang BS (2014) Comparative numerical analysis of sheet formed into a V-shaped die using conventional and electromagnetic forming processes. *Adv Mech Eng* 6:240789
9. Liu W, Zou XF, Huang SY, Zhu J, Lei Y (2018) Numerical simulation of collision effect on damage evolution in electromagnetic forming of aluminum alloy sheet. *Key Eng Mater* 765:216–221
10. Kamal M, Daehn GS (2007) A uniform pressure electromagnetic actuator for forming flat sheets. *J Manuf Sci Eng* 129:369–379
11. Golowin S, Kamal M, Shang J, Portier J, Din A, Daehn GS, Bradley JR, Newman KE, Hatkevich S (2007) Application of a uniform pressure actuator for electromagnetic processing of sheet metal. *J Mater Eng Perform* 16:455–460
12. Thibaudeau E, Kinsey BL (2015) Analytical design and experimental validation of uniform pressure actuator for electromagnetic forming and welding. *J Mater Process Technol* 215:251–263
13. Meng Z, Huang S, Huang W, Hu J, Xia Z (2011) Effects of process parameters on warm and electromagnetic hybrid forming of magnesium alloy sheets. *J Mater Process Technol* 211:863–867
14. Feng F, Huang S, Hu J, Meng Z, Lei Y (2013) Analysis of the bulging process of an AZ31B magnesium alloy sheet with a uniform pressure coil. *Int J Adv Manuf Technol* 69:1537–1545
15. Xu J, Zhou Y, Cui J, Huang L, Zhang X, Li G (2018) Effects of temperature and driver sheet for magnesium alloy sheet in magnetic pulse forming. *Int J Adv Manuf Technol* 95:3319–3333
16. Kim JH, Kim D, Lee MG (2015) Experimental and numerical analysis of a rectangular helical coil actuator for electromagnetic bulging. *Int J Adv Manuf Technol* 78:825–839
17. Shang J, Daehn G (2011) Electromagnetically assisted sheet metal stamping. *J Mater Process Technol* 211:868–874
18. Liu W, Zou X, Huang S, Lei Y (2018) Electromagnetic-assisted calibration for surface part of aluminum alloy with a dedicated uniform pressure coil[J]. *Int J Adv Manuf Technol* 100:721–727
19. Livermore Software Technology Corp. (2018) LS-DYNA® keyword user's manual volume II material models
20. Noh HG, Lee K, Kang BS, Kim J (2016) Inverse parameter estimation of the Cowper-Symonds material model for electromagnetic free bulge forming. *Int J Precis Eng Manuf* 17(11):1483–1492

Publisher's note Springer Nature remains neutral with regard to jurisdictional claims in published maps and institutional affiliations.